

# Design and Implementation of LVDC Hybrid Circuit Breaker

Riccardo Lazzari\*, Luigi Piegari\*\*

\* Power Generation Technologies and Materials Department, RSE, Milan, Italy

\*\* Department of Electronics, Information and Bioengineering, Politecnico di Milano, Milan, Italy

**Abstract** - In recent years, DC distribution grids have become increasingly popular because of the interest in the diffusion of distributed renewable energy. In this scenario, DC distribution grids are also favored because of the increased use of batteries and power electronic loads. The main limit to the spread of DC grids is their protection devices, which still present several problems. At present, protection devices are represented by traditional mechanical breakers or static electronic components. The first, which interrupt DC currents, have good reliability but need maintenance and have long intervention periods. In contrast, electronic switches are fast and reliable, but they reduce the efficiency because of their voltage drop. In this scenario, some hybrid breakers have been proposed to obtain the advantages of both devices. **The previous solutions of hybrid breakers still suffer several critical issues and, usually, are not capable of protecting a system from short circuits without significantly reducing their lifetime.** In this paper, a new low-voltage hybrid circuit breaker topology is proposed. The procedure to dimension all of the active and passive components in the device is analyzed, and the effectiveness of the proposed solution is proven by means of experimental results obtained using a prototype.

**Index terms** – DC Circuit breakers, Hybrid circuit breaker, LVDC breakers, Protection devices, Fast circuit breakers

## **Luigi Piegari**

Department of Electronics, Information and Bioengineering– Politecnico di Milano

Piazza Leonardo da Vinci 32, Milan, Italy

Tel. +39 02 23994125

Email: luigi.piegari@polimi.it

# Design and Implementation of LVDC Hybrid Circuit Breaker

## Abstract

In recent years, DC distribution grids have become increasingly popular because of the interest in the diffusion of distributed renewable energy. In this scenario, DC distribution grids are also favored because of the increased use of batteries and power electronic loads. The main limit to the spread of DC grids is their protection devices, which still present several problems. At present, protection devices are represented by traditional mechanical breakers or static electronic components. The first, which interrupt DC currents, have good reliability but need maintenance and have long intervention periods. In contrast, electronic switches are fast and reliable, but they reduce the efficiency because of their voltage drop. In this scenario, some hybrid breakers have been proposed to obtain the advantages of both devices. **The previous solutions of hybrid breakers still suffer several critical issues and, usually, are not capable of protecting a system from short circuits without significantly reducing their lifetime.** In this paper, a new low-voltage hybrid circuit breaker topology is proposed. The procedure to dimension all of the active and passive components in the device is analyzed, and the effectiveness of the proposed solution is proven by means of experimental results obtained using a prototype.

## 1. Introduction

Nowadays, the technological progress in the power conversion field and the wide diffusion of renewable energy sources (RES) are promoting the implementation of DC distribution grids. This is a growing trend mainly due to the advantages offered by DC grids when compared to AC grids in many applications (e.g., data centers, marine installations, and offshore wind farms) [1]-[6].

However, the implementation of a DC network introduces a complex mix of power converters with significant technical challenges in order to protect and operate the system. DC converters require capacitance filters to mitigate the voltage ripples, but if a DC bus short circuit occurs, the capacitors rapidly discharge into the fault, causing a current surge with an amplitude that depends on the filter design and location of the fault [7]. For boost converters, when the capacitor voltage drops, the antiparallel diodes of the converters will be forward biased, which will continue to supply the fault [8]. This occurs in addition to the issue of interrupting a DC current without natural zero crossing points, which is typical for AC systems. In this situation, it is essential to develop well-designed protection to ensure the reliable operation of a DC microgrid.

The development of an advanced protection scheme requires the design and implementation of circuit breakers (CBs) able to isolate the faulty section in several milliseconds [9], [10] to prevent any damage. The basic requirements for a circuit breaker are

- i) the ability to handle large currents with low losses;

- ii) a fast transition time from conduction to a blocking state without stress during breaking;
- iii) a high dielectric strength to block the current against a high potential at its terminal [11]-[13].

However, there are many challenges to design a DC circuit breaker due to the absence of zero crossing in the DC current and the low inductance of a DC system, which leads to a very high rise rate for the fault current [14].

Traditional mechanical circuit breakers (MCBs) are compliant with the first and third requirements, but they have a slow transition time because of the need to blow the arc in **extinguishing chamber**. The manipulation of the arc to move it into the arc chute, where it can be extinguished quickly and reliably is, perhaps, the most difficult aspect when designing DC MCBs [15].

On the other hand, solid state circuit breakers (SSCBs) are able to commutate from the conduction to the blocking state in a few microseconds [16]. Moreover, because of the absence of moving parts, SSCBs do not suffer phenomena like arcing, contact erosion, and bounce. This is a clear advantage offered by SSCBs, but in the realization of this kind of breaker, it is necessary to add other elements such as metal oxide varistors (MOVs) or snubber circuits [17] to absorb the magnetic energy stored in the system inductance [18]. Otherwise, the overvoltage peak during turn-off may damage power semiconductor devices and other components in the DC grid. In the same way, during a fault condition, overcurrent peaks may damage power semiconductor devices. Furthermore, the on-state resistance of the power electronic switches causes power losses and heating that must be dissipated through a well-suited cooling system. For these reasons, the applications of SSCBs are strictly limited to applications where the fault currents are limited to a fixed rate, a fast off-transition is the essential requirement, and the losses are manageable.

There has been significant interest in combining a MCB with power semiconductor devices to configure so-called hybrid circuit breakers (HCBs) [19], [20]. A HCB combines the very low resistance of an MCB in the on-state with the fast and arc-less transition from the conduction to the blocking state of an SSCB. To do that, a parallel MCB and SSCB combination is used to reduce the arc, which cannot be avoided in the MCB [21]. In general, it is possible to resort to two main techniques: Zero-Voltage Switching (ZVS) and Zero-Current Switching (ZCS) [22]. In the first case, the voltage across the MCB is maintained close to zero during the separation of the contacts, while, in the second case, the current in the MCB is forced to zero before turning the device off.

In [23], the authors presented a ZVS HCB where a power field-effect transistor (FET) was connected in parallel to an MCB and energy absorber. Under normal conditions, the current flows through the MCB, while in the case of a fault, the main contacts of the MCB are opened, and the FET is turned on. When the current level and arc impedance reach an appropriate level, the current flows in the FET, which can finally interrupt this current. The same operation was also used in [24]-[26], where the current commutation to the SSCB was actuated by the arc generated between the contacts

of the MCB during the off-transition. However, the arc causes erosion of the contacts, resulting in a shorter lifetime and need for maintenance.

To solve the problem of the arc needed for the commutation in the SSCB branch, in [27], the authors proposed the use of an auxiliary commutating switch comprised of one or more semiconductors in series with the MCB. During normal operation, the current flows through an auxiliary commutating switch and MCB in series. When the commutating switch is turned off, the current is quickly diverted to the parallel SSCB, and the MCB can be opened with zero-current. In this situation, the power dissipation under normal operation is **higher** than that of a conventional MCB due to the semiconductor auxiliary switch. For this reason, in [28] and [29], the authors proposed the use of a low-voltage MOSFET-based commutating switch, composed of a high parallel number of power semiconductor devices, in order to reduce the losses. However, to maintain low commutation losses, a MOSFET with a low breakdown voltage must be chosen. Therefore, the SSCB **can** be opened only after the MCB to avoid applying the voltage across the hybrid DC breaker to the commutating switch. The realization of such a device and its snubber circuit is not an easy task [27]. In addition, the SSCB must be designed to handle all of the fault current as long as the MCB is open.

Otherwise, the use of ZCS HCBs may avoid the turn-off arcing phenomenon through the use of additional resonant components, which allow the reduction of the MCB current to zero. In [30], the authors proposed a ZCS structure where the main components were a fast MCB opened by an electrodynamic repulsion force, a pre-charged capacitor, two thyristors, and a voltage suppressor. To interrupt a current, one of the thyristors is turned-on, causing the discharge of the capacitor in the opposite direction of the main current and flowing through the MCB. In this way, the current is reduced, and the mechanical contact can be opened at a fast rate with limited arcing. This HCB is one of the most effective presently available low voltage current-limiting and interrupting devices [20], but has some disadvantages like an overvoltage on the load after the MCB opens, the impossibility of reducing the current to zero during a fault, and the necessity of an external circuit to pre-charge the capacitor.

To solve all these problems, this research aimed to develop a ZCS HCB that is able to switch-off the circuit during normal operation and during fault condition to avoid an overcurrent and overvoltage on the breaker and DC grid components. The proposed structure can also open on a short circuit using its internal inductances to partially limit the current increase. Moreover, it has a reclosing path for the current to avoid overvoltage on the components. Finally, it integrates all of the necessary devices to pre-charge its capacitor and quickly detect fault conditions.

## **2. Topology and working principle**

The basic principle of operation of the proposed DC breaker is explained in the following. In the basic scheme, reported in Fig. 1,  $T$  is a traditional mechanical breaker, while  $S_1$  and  $S_2$  are two switching devices (i.e., IGBT or MOSFET).

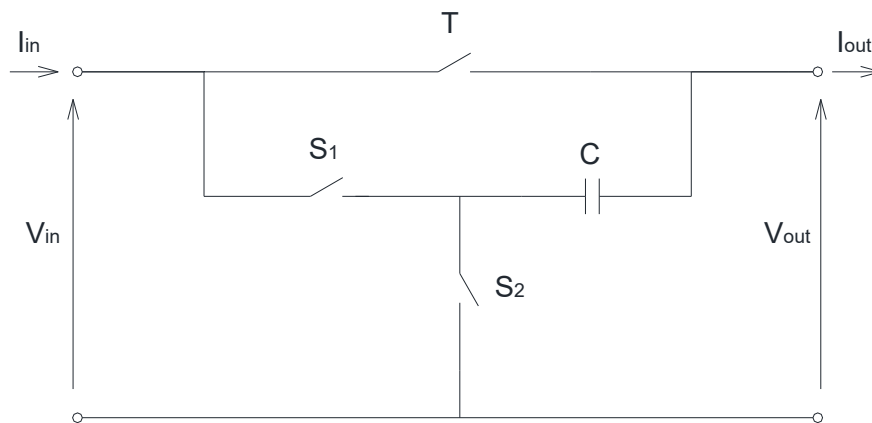


Fig. 1. Basic scheme of proposed DC breaker

During normal operation in conduction mode,  $T$  and  $S_2$  are closed, while  $S_1$  is in an open state. In this way, the capacitance  $C$  is charged to the supply voltage. In order to open the breaker,  $S_1$  and  $S_2$  are switched on and off, respectively (introducing the necessary dead-time). **In this way, capacitor  $C$  will force the current in  $T$  to zero and then change its direction.** If  $T$  opens its contacts when the current crosses zero, no arc arises. Then, switch  $S_1$  can be opened, interrupting the load current.

The main goal of the proposed hybrid DC breaker is to achieve:

1. High efficiency;
2. Long lifetime;
3. The ability to open under a short circuit (for the maximum interruption power) without damage.

**Point 1 is achieved, by the topology of the breaker shown in Fig. 1, as long as the parasitic resistance in the mechanical breaker  $T$  is sufficiently low.** In normal operation, the current flows in mechanical device  $T$  with negligible voltage drop and power loss. In order to achieve point 2, it is necessary that the opening phases of  $T$  are operated at a very low current (possibly in the absence of an arc). With the basic configuration of Fig. 1, it is not possible to ensure this condition. Indeed, when  $S_1$  is turned on (and  $S_2$  is turned off), the current in  $T$  quickly becomes negative, making it practically impossible to open with a near zero-current. In order to slow down the current inversion, an inductance,  $L$ , is introduced in the scheme in series with the mechanical device  $T$ . Moreover, by closing  $S_1$ , capacitance  $C$  is put in series with the voltage source. For this reason, a voltage that is double the rated one is instantaneously connected to the load, which could cause damage. For this reason, an output inductance,  $L_{out}$ , is used to limit the overvoltage on the load when the breaker opens. The next section will show that the correct sizing of the two inductances allows a current limitation during short circuit for the time necessary to open the circuit. This makes possible the achievement of point 3, allowing the breaker to open, under a short circuit condition, before the current becomes too high to be interrupted by  $S_1$ . In order to quickly identify the fault condition, an output capacitance,  $C_{out}$ , is added to provide a high fault current while the output inductor current is still low. The complete circuit of the proposed breaker is reported in Fig. 2. **The parasitic**

resistances of the two inductances,  $L$  and  $L_{out}$ , during normal operation cause additional losses. This point will be addressed as part of the experimental analysis, in section 5.c, where it is shown that losses during normal operation are significantly lower than an all-electronic breaker.

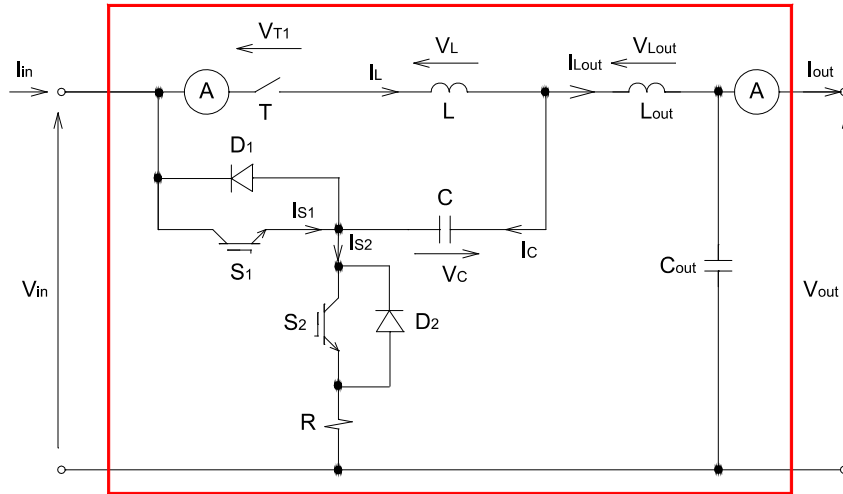


Fig. 2. Complete scheme of proposed circuit breaker

Looking at the scheme of Fig. 2, three other elements can be noted: the resistance  $R$  and the two diodes,  $D_1$  and  $D_2$ . Resistance  $R$  is necessary to dissipate the energy stored in capacitance  $C$  in the case of a short circuit. When  $S_1$  completes the opening phase of the breaker, capacitance  $C$  is still charged. It discharges on the load by means of diode  $D_2$ . In the case of a short circuit, a current limitation can be achieved by means of the proper sizing of  $R$ , as discussed in section 3. When the breaker is energized, the presence of the capacitance,  $C$ , could cause an overload on the voltage source. In order to limit the charge current, a PWM modulation technique is performed on switch  $S_2$  using inductance  $L$  to limit the current ripple. During PWM, when  $S_2$  is turned off, the inductive current closes in diode  $D_1$ , avoiding overvoltage on the two electronic switches.

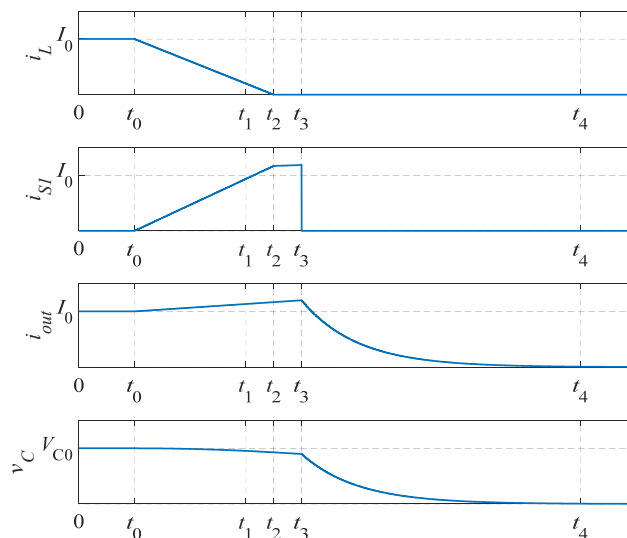


Fig. 3. Working principle of proposed circuit breaker

The complete working principle of the breaker is illustrated in Fig. 3 and summarized in the following:

**[ $t_0$ - $t_1$ ]:** at time  $t_0$ , the control system decides to open. This could be driven by an opening request from the operator or from a short circuit detection. At  $t_0$ , switch  $S_2$  is opened and, after the necessary dead time,  $S_I$  is closed. The current in  $S_I$  starts increasing while the current in  $L$  starts decreasing. If capacitance  $C$  is large enough, its voltage is almost constant during this time, and the currents in both  $S_I$  and  $L$  change linearly. At time  $t_1$ , the current in  $L$  reaches a low current threshold, for which the opening of  $T$  can be started.

**[ $t_1$ - $t_2$ ]:** at time  $t_1$ , the opening command to  $T$  is sent.  $T$  starts opening, and its current reaches zero at time  $t_2$ . During this time interval, nothing changes in the circuit.

**[ $t_2$ - $t_3$ ]:** after opening the breaker, an additional time interval,  $t_2$ - $t_3$ , is introduced before opening  $S_I$ . The reason for this delay is that the time needed for the MCB to open could slightly change with ageing. During this time, the current in  $S_I$  becomes equal to the output current and increases slower than in the previous intervals.

**[ $t_3$ - $t_4$ ]:** at time  $t_3$ , switch  $S_I$  is turned off. Capacitance  $C$  discharges itself on the load with a time constant depending on the series of the load resistance and breaker resistance  $R$ . After 5 times the time constant, the transient can be considered terminated, and the circuit can be considered turned off.

In practical implementation, the mechanical breaker requires a not negligible time to open its contacts. In particular, a delay occurs between the instant when the opening command is generated and the instant in which the contacts are detached. If this period is known (for example by means of experimental measurements), it is possible to anticipate the command signal of the mechanical breaker, and the working principle remains unchanged. Unfortunately, this delay is not constant but can vary from a minimum to a maximum value in the lifetime of the mechanical breaker. For this reason, a slight modification of the control strategy is implemented in order to keep all the advantages of the proposed solution. In particular, calling  $t_d$  the minimum delay, the opening signal of the mechanical device is anticipated by  $t_d$ . As a consequence, when the current in the mechanical device becomes zero, the contacts do not open yet and, therefore, the currents become negative and start increasing in the opposite direction. In order to avoid the need to interrupt a high negative current,  $S_I$  is controlled with a hysteresis band to keep the current in a predefined bandwidth around zero. In this way, when the contacts of the mechanical device open, they have to interrupt a very low current.

### 3. Sizing procedure

This section proposes a sizing procedure for the passive components of the suggested circuit breaker. The components to be sized are the two inductances,  $L$  and  $L_{out}$ , the capacitance,  $C$ , and the resistance,  $R$ . At the end of this section, some considerations about the sizing of the switching components will also be given.

In order to correctly size the components, it is possible to analyze the circuit during the opening phase. In the scheme reported in Fig. 4, the output capacitance has been neglected because, as stated above, it is a small capacitance necessary only for tripping purposes.

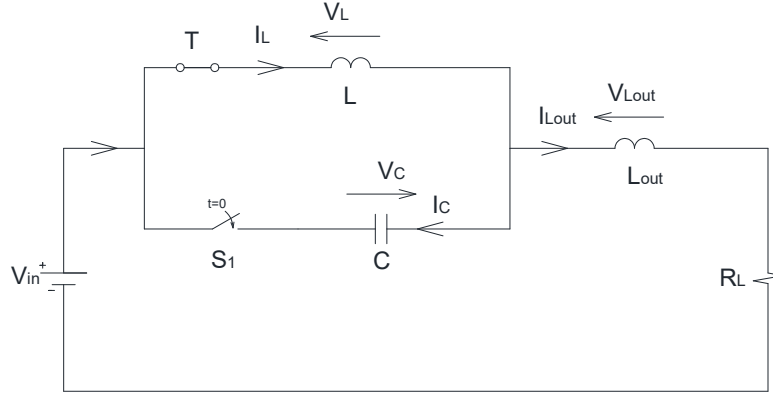


Fig. 4. Electric circuit during opening

The resistive load, indicated by  $R_L$ , could represent the short circuit resistance, in the case of opening in a fault condition. The transient can be analyzed by applying the Kirchhoff laws:

$$\begin{cases} V_{in} = L \frac{di_L}{dt} + L_{out} \frac{di_{L_{out}}}{dt} + R_L i_{L_{out}} \\ V_C + L \frac{di_L}{dt} = 0 \\ i_L = i_{L_{out}} + C \frac{dV_C}{dt} \end{cases} \quad (2)$$

Easily, eq. (2) can be summarized in

$$V_{in} = L_{out} LC \frac{d^3 i_L}{dt^3} + R_L LC \frac{d^2 i_L}{dt^2} + (L + L_{out}) \frac{di_L}{dt} + R_L i_L \quad (3)$$

The system is a third order system, and it cannot be solved in a closed form. In any case, the worst condition occurs during faults with low impedance. In this case, it is possible to neglect the terms in which  $R_L$  appears, and eq. (3) can be rewritten as follows:

$$V_{in} = L_{out} LC \frac{d^3 i_L}{dt^3} + (L + L_{out}) \frac{di_L}{dt} \quad (4)$$

Considering that at the beginning of the phenomenon, the inductive currents are equal to the healthy load current and the capacitance voltage is equal to the source voltage, the initial conditions to be coupled to (4) can be calculated as follows:



$$\begin{cases} i_L(0) = \frac{V_{in}}{R_n} \\ \frac{di_L}{dt}(0) = \frac{V_L(0)}{L} = -\frac{V_C(0)}{L} = -\frac{V_{in}}{L} \\ \frac{d^2i_L}{dt^2}(0) = \frac{1}{L} \frac{dV_L}{dt}(0) = -\frac{1}{L} \frac{dV_C}{dt}(0) = -\frac{1}{LC} i_C(0) = -\frac{1}{LC} [i_L(0) - i_{L,out}(0)] = 0 \end{cases} \quad (5)$$

where  $R_n$  indicates the load resistance before the fault. Taking into account (5), the solution of (4) can be written in the following form:

$$i_L(t) = \frac{V_{in}}{R_n} + \frac{V_{in}}{L+L_{out}} t - \frac{V_{in}(2L+L_{out})}{L(L+L_{out})} \sqrt{\frac{LL_{out}C}{L+L_{out}}} \sin\left(\sqrt{\frac{L+L_{out}}{LL_{out}C}} t\right) \quad (6)$$

The current given by (6) increases linearly with some smoothed sinusoidal oscillation, as illustrated in Fig. 5.

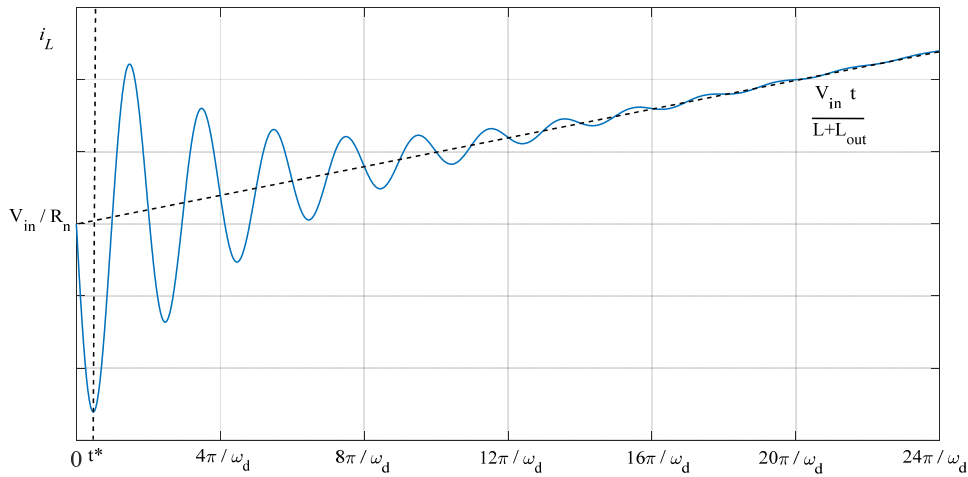


Fig. 5. Trend for the current as given by eq. (6)

In order to allow the inversion of the current in the mechanical component  $T$ , it is necessary that the first minimum of the function is lower than zero. This condition is expressed by (7).

$$t^* = \frac{\pi}{2} \sqrt{\frac{LL_{out}C}{L+L_{out}}} \quad (7)$$

$$i_L(t^*) = \frac{V_{in}}{R_n} + \frac{V_{in}}{L+L_{out}} \frac{\pi}{2} \sqrt{\frac{LL_{out}C}{L+L_{out}}} - \frac{V_{in}(2L+L_{out})}{L(L+L_{out})} \sqrt{\frac{LL_{out}C}{L+L_{out}}} < 0$$

From inspecting the second part of (7), it is clear that the input voltage has no effect on the possibility to invert the current. This condition can be ensured with the proper sizing of the passive components. Eq. (7) can be rewritten as follows:

$$\left(2 - \frac{\pi}{2}\right)^2 + \left(\frac{L_{out}}{L}\right)^2 + (4 - \pi) \frac{L_{out}}{L} > \frac{(L+L_{out})^3}{R_n^2 LL_{out}C} \quad (8)$$

Then, considering a new variable,  $x$ , given by the ratio between  $L_{out}$  and  $L$  the result is the following:

$$x = \frac{L_{out}}{L}$$

$$f(x) = (R_n^2 C - L)x^3 + [R_n^2 C(4 - \pi) - 3L]x^2 + \left[ R_n^2 C \left( 2 - \frac{\pi}{2} \right)^2 - 3L \right]x - L > 0 \quad (9)$$

The function  $f(x)$  is a cubic whose limit for  $x$  that goes to infinite has the sign of the first term. For this reason, a solution always exists if it is

$$R_n^2 C - L > 0 \quad \Rightarrow \quad \frac{L}{C} < R_n^2 \quad (10)$$

If all the coefficients of the polynomial function  $f(x)$  are positive, but the last one  $f(x)$  is an increasing monotone function and, over a fixed value of  $x$ , the second of (9) is always verified. In order to have all the coefficients of the second part of (9) positive it has to be

$$R_n^2 C(4 - \pi) - 3L > 0 \quad \Rightarrow \quad \frac{L}{C} < \frac{R_n^2(4 - \pi)}{3} \quad (11)$$

For each value of  $L/C$ , it is possible to obtain the minimum value of the ratio  $L_{out}/L$  allowing the inversion of the current in  $T$ . The results are reported in Fig. 6.

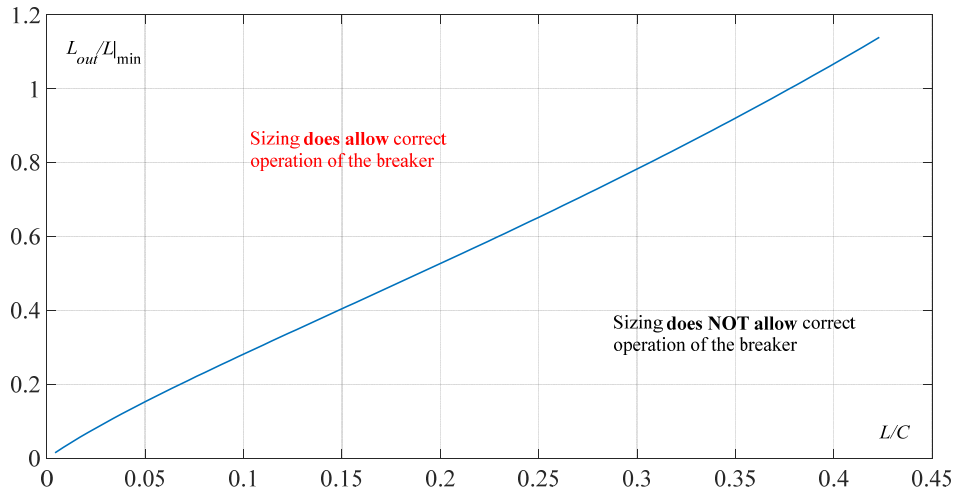


Fig. 6. Minimum ratio  $L_{out}/L$  versus ratio  $L/C$  for correct operation of breaker

The sizing of the passive components also has to take into account the maximum current in switch  $S_I$ . Indeed,  $S_I$  has to be capable of conducting and interrupting the current without **failing**. As discussed in section 2, the current in  $S_I$  increases differently in the two intervals  $[t_0-t_2]$  and  $[t_2-t_3]$ . According to Fig. 3, in the first of the two intervals, it increases with a high slope, the sum of the slopes of  $-i_L$  and of  $i_{out}$ , while in the second interval, it increases with the slope of  $L_{out}$ . At the end of the first interval, it reaches the value  $I_0$ , which is the current of the mechanical device when  $S_I$  is turned on. It is worth noting that, if the breaker is operating in a faulty condition, during the time delay  $t_d$ , the current in the mechanical device increases almost linearly, limited by the two inductances  $L$  and  $L_{out}$  in series. During

this transient, we can consider the voltage across the capacitance to be constant, and for a zero load voltage (short circuit) it is found as follows:

$$\begin{cases} \frac{di_{S_1}}{dt} = -\frac{di_L}{dt} + \frac{di_{L_{out}}}{dt} \approx \frac{V_{in}}{L} + \frac{2V_{in}}{L_{out}} & t \in [t_0 - t_2] \\ \frac{di_{S_1}}{dt} = \frac{di_{L_{out}}}{dt} \approx \frac{2V_{in}}{L_{out}} & t \in [t_2 - t_3] \end{cases} \quad (12)$$

The maximum current in the switching device is reached at time  $t_3$  and it is found as follows:

$$I_{S_1, \max} = I_0 + \frac{2V_{in}}{L_{out}}(t_3 - t_2) \quad (13)$$

As mentioned above, in the case of a short circuit, during the time delay  $t_d$ , the current in the mechanical device increases almost linearly, and it results in the following:

$$I_0 = I_{Load} + \frac{V_{in}}{L + L_{out}}t_d + \frac{2V_{in}}{L_{out}}(t_2 - t_0) \quad (14)$$

Combining (14) and (15) results in the following:

$$I_{S_1, \max} = I_{Load} + \frac{V_{in}}{L + L_{out}}t_d + \frac{2V_{in}}{L_{out}}(t_3 - t_0) \quad (15)$$

Equation (15) was obtained by assuming that the voltage across the capacitance during the considered operation time is constant. In order to verify if this hypothesis can be considered valid, the voltage drop is estimated.

Because the current in the capacitance is equal to the current in  $S_1$ , the variation of the voltage across the capacitance can be estimated as follows:

$$\begin{aligned} \Delta V_c &= V_{in} - V_c(t_3) = \frac{1}{C} \left\{ \int_{t_0}^{t_2} \left( \frac{V_{in}}{L} + \frac{2V_{in}}{L_{out}} \right) (t - t_0) dt + \int_{t_2}^{t_3} \left[ \left( \frac{V_{in}}{L} + \frac{2V_{in}}{L_{out}} \right) (t_2 - t_0) + \frac{2V_{in}}{L_{out}} (t - t_2) \right] dt \right\} = \\ &= \frac{1}{C} \left\{ \left( \frac{V_{in}}{L} + \frac{2V_{in}}{L_{out}} \right) \frac{1}{2} \Delta t_2^2 + \int_{t_2}^{t_3} \left[ \left( \frac{V_{in}}{L} \right) (t_2 - t_0) + \frac{2V_{in}}{L_{out}} (t - t_0) \right] dt \right\} = \\ &= \frac{1}{C} \left\{ \left( \frac{V_{in}}{L} + \frac{2V_{in}}{L_{out}} \right) \frac{1}{2} \Delta t_2^2 + \left( \frac{V_{in}}{L} \right) \Delta t_2 (\Delta t_3 - \Delta t_2) + \frac{V_{in}}{L_{out}} (\Delta t_3^2 - \Delta t_2^2) \right\} = \\ &= \frac{1}{C} \left\{ \frac{V_{in}}{L} \Delta t_2 \left( \Delta t_3 - \frac{\Delta t_2}{2} \right) + \frac{V_{in}}{L_{out}} \Delta t_3^2 \right\} \end{aligned} \quad (16)$$

with

$$\begin{aligned} \Delta t_2 &= t_2 - t_0 \\ \Delta t_3 &= t_3 - t_0 \end{aligned} \quad (17)$$

According to (17),  $\Delta t_2$  and  $\Delta t_3$  represent the time necessary to bring the current to zero in the mechanical device and the time necessary to have the contacts of the breaker far enough apart.

Finally, in order to have a voltage variation on the capacitance lower than a maximum value  $\Delta V_{C,\max}$ , it has to be as follows:

$$C > \frac{V_{in}}{\Delta V_{C,\max} L} \Delta t_2 \left( \Delta t_3 - \frac{\Delta t_2}{2} \right) + \frac{10}{L_{out}} \Delta t_3^2 \quad (18)$$

Equations (18) and (15) and Fig. 6 give the necessary information to size all the components of the device. An example is reported in the next section, in which the real prototype is analyzed.

It is worth noting that if inductances with iron cores are used, saturation could occur during short circuit. In this case, the global inductance would decrease affecting the correct operation of the breaker in short circuit opening. A correct sizing of the inductances should take into account this aspect.

#### 4. Experimental test setup

The capabilities of the proposed hybrid circuit breaker were verified through experimental activities carried out on the prototype shown in Fig. 7. The components of the prototype were chosen by considering a nominal voltage of 200 V, nominal current of 20 A, and maximum value of 400 A for the current of the component  $S_1$ .



Fig. 7. Photo of hybrid DC circuit breaker prototype

The DC contactor Tyco EV200AAANA was used to realize the prototype. This component, as reported in the datasheet, has a release time (arcing included) equal to 12 ms. In our prototype, the extinguishment of the arc was performed by the suggested structure, and so some preliminary experiments were carried out on the mechanical breaker

to evaluate the release time before the arc. The opening time was typically equal to 3.7 ms. Taking into account this information, it was possible to calculate the values of the two inductances  $L$  and  $L_{out}$ , which satisfied (15). In particular, considering a ratio between  $L_{out}$  and  $L$  equal to  $k$ , it is possible to write the following:

$$L = \frac{V_{in}kt_d + 2V_{in}(k+1)\Delta t_3}{(I_{S1,max} - I_{Load})k(k+1)} \quad (19)$$

Considering an on-state duration for the component  $S_1$ ,  $\Delta t_3 = 100 \mu s$ , load current  $I_{load} = 20$  A; maximum current in  $S_1$ ,  $I_{S1,max} = 400$  A; and DC voltage  $V_{in} = 200$  V, through (19) it was possible to draw the graph of Fig. 8 considering different values for ratio  $k$ .

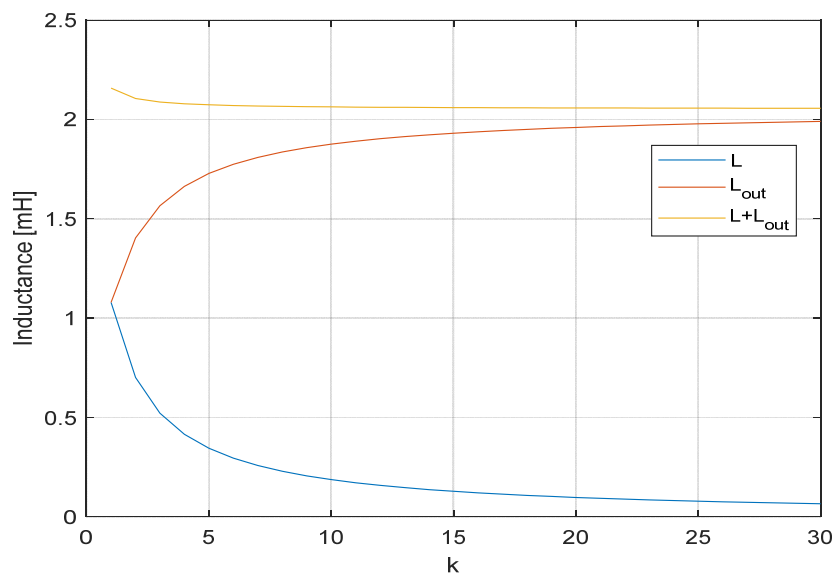


Fig. 8. Trend of inductance values to maintain  $I_{S1} < 400$  A with input voltage of 200 V in presence of short circuit

Therefore, to satisfy this requirement, it is necessary for the total inductance to be about 2 mH. In the realization of the prototype, an inductance  $L$  of 400  $\mu H$  and inductance  $L_{out}$  of 1.8 mH were chosen. These inductances modify the behavior of the overall DC grid increasing the total line inductance and reducing the oscillation frequency. In particular, eigenvalues approach the imaginary axis from the left half-plane, decreasing the stability margin of the system. This issues can be approached through the design of the current and voltage controller of the converters in accordance with the stability analysis of the overall grid [31], [32]. However, the use of inductors can limit fault current rating, preventing the fault current to reach the blocking level in the converter and enable the discrimination of the faults in fast protection methods, like ROCOV [33].

It is worth noting that the necessity of big inductances is due to the use of a mechanical breaker spending almost 4ms to open its contacts. By using faster mechanical breakers (that have to work with low currents) the inductances and

thereby the losses can be strongly reduced. Fast mechanical DC breakers are under study in recent years and some prototypes, capable of opening in time windows shorter than 4ms are presented in [34] and [35].

Starting from the inductances, it was possible to evaluate capacitance  $C$  and find a value that satisfied both (10) and (18). Taking into account a maximum voltage variation  $\Delta V_{C,\max} = 10\%$ , the minimum capacitance was equal to 4 mF, and in the realization of the prototype, a 9.6 mF capacitance was used.

The dimensioning procedure has been set up with a zero fault resistance, so that, for any fault resistance the current is limited by the inductances into a range of correct operability of the device. Nevertheless, if the fault resistance is very low the initial current, supplied by the output capacitor, could persist over the threshold for a time too short to allow a correct detection. In order to avoid this problem a correct dimensioning of the output capacitance has to be performed. In particular, the output capacitance must ensure that the current, after one control period is still higher than the threshold. Considering a resistive short circuit whose value is  $R_f$ , neglecting the current supplied by the output inductance, the fault current can be written as:

$$I_{out} = \frac{V_{in}}{R_f} e^{-\frac{t}{R_f C_{out}}} \quad (20)$$

Imposing that after a control time the output current is higher than the threshold implies:

$$\begin{aligned} \frac{V_{in}}{R_f} e^{-\frac{T_s}{R_f C_{out}}} &> I_{th} \\ \frac{T_s}{R_f C_{out}} &< -\ln\left(I_{th} \frac{R_f}{V_{in}}\right) \\ C_{out} &> \frac{T_s}{R_f \ln\left(\frac{V_{in}}{R_f I_{th}}\right)} \end{aligned} \quad (21)$$

In the prototype the output capacitance was dimensioned to open a short circuit of 10 kA corresponding to a fault resistance equal to 20 m $\Omega$ . The capacitance resulting from the third relation of the (21), considering the parameter of the experimental setup, is 97  $\mu$ F and a 100  $\mu$ F was used in the prototype. In Fig. 9 the  $I_{out}(T_s)$ , evaluated using the (20), is compared with the current threshold for different fault resistances with an output capacitance equal to 100  $\mu$ F. It is clear that, with the used capacitance, the fault can be identified until a minimum resistance around 19.4 m $\Omega$  (according with the (21)).

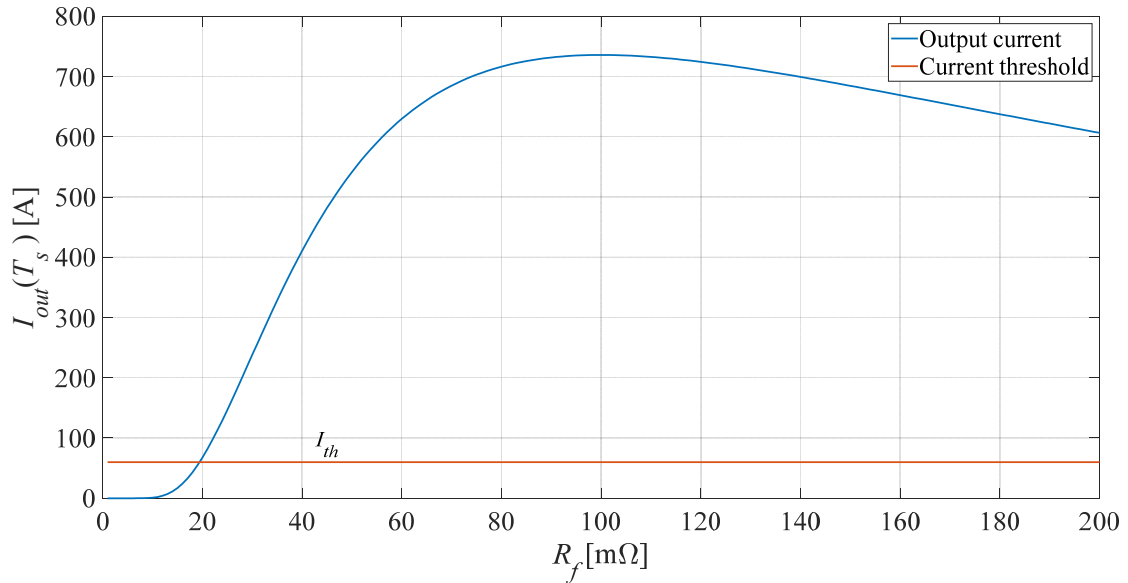


Fig. 9. Output current after one control period versus fault resistance

It is worth noting that the presence of a big inductance in the fault could slightly change the behavior of the proposed breaker. Indeed, for the presence of the fault inductance the initial peak current could not go over the threshold, triggering the opening of the breaker. In this case, the fault would be identified only when the current in  $L_{out}$  reaches the threshold. The slope of the current in this case would be lower because the fault inductance is in series with the output inductance of the breaker and, therefore, the two effects compensate themselves. A complete analysis of this phenomenon is not in the focus of the paper and will be addressed in future works. The parameters of all the components of the HCB are reported in Table 1.

Table 1 Hybrid DC circuit breaker parameters

Component	Specification
<b>Mechanical Breaker T</b>	Tyco EV200AAANA
<b>Switch S1 &amp; S2</b>	Semikron SKM400GB12T4
$C$	9.6 mF
$L$	400 μH
$C_{out}$	100 μF
$L_{out}$	1.8 mH
$R$	0.5 Ω

The prototype was equipped with two current sensors (LEM HAS 400-S), connected as shown in Fig. 2, and one voltage sensor (LEM LV 25-1000), which was necessary for the pre-charge of  $C$ . All these measurements were used by a microcontroller Texas Instruments TMS320F28335PGFA to control the HCB consisting of the mechanical breaker

and electronic switches. The realized firmware had a cycle time of  $10\ \mu\text{s}$ , and during this time it acquired the output current and eventually activated the start-up or opening procedure if the switching button was pressed by the operator or the current was higher than a fixed threshold. The start-up procedure was realized by closing breaker  $T$  and then activating the pre-charge of capacitor  $C$ . This was done through electronic switch  $S_2$ , which was controlled through a hysteresis control on the capacitor current. When the voltage on capacitor  $C$  reached 90% of the input voltage, this procedure finished, and switch  $S_2$  remained closed. During the opening procedure, which could be caused by an external command or a fault detection (the current threshold was set equal to 60 A for the prototype), the control after a delay equal to 3.2 ms sent the trip command to mechanical breaker  $T$ , turn-off command to  $S_2$ , and switching command to component  $S_1$ . The switching command for component  $S_1$  was realized through the use of a hysteresis control to maintain the mechanical breaker current close to zero. After a delay of 3 ms, component  $S_1$  was turned off. In this situation, the load was supplied only by capacitor  $C$ , which was discharged.

## 5. Experimental results

The experimental validation of the proposed hybrid circuit breaker was performed using the DC microgrid of RSE [36] at a constant voltage of 200 V and connecting the HCB to a dedicated resistive load of  $11\ \Omega$ . In this study, the experimental activity is focused to verify the ability of the proposed HCB during load interruption and fault interruption with a limited fault current. In particular, a short circuit fault was simulated with a resistance of  $2\ \Omega$ . In order to increase the current capacity during the fault, a bank of supercapacitors was installed in parallel with the voltage generator during the test. In the test, an oscilloscope (Tektronix DPO3014) equipped with two voltage probes (Tektronix P5200) was used. For the current measurements, the oscilloscope was directly connected to the current sensor (LEM HAS 400-S) of the prototype. In Fig. 10 the experimental test setup with indicated measurement points is shown.

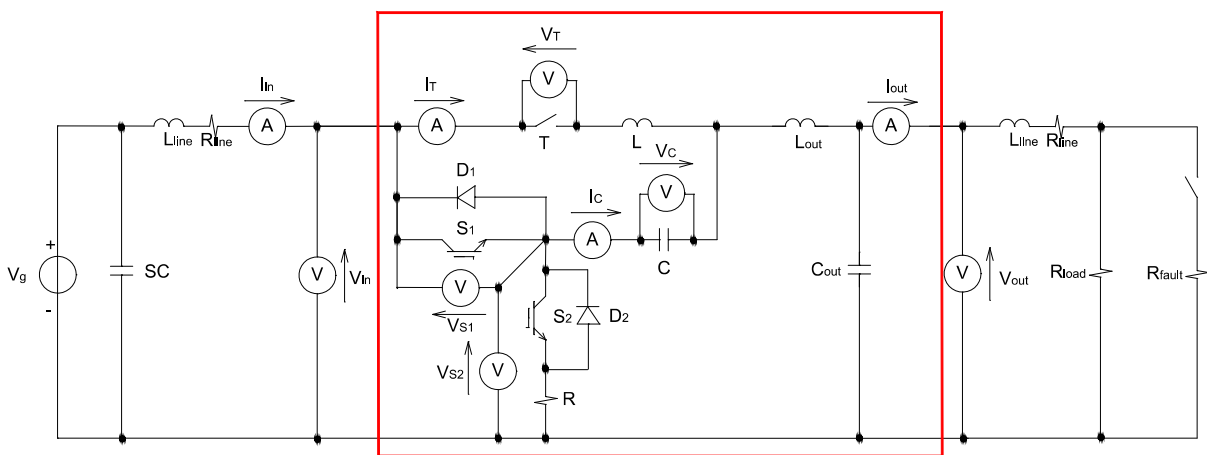


Fig. 10. Experimental Test Setup



### a. Resistive load interruption test

The performance of the HCB was first verified during a resistive load interruption. Fig. 11 shows the current and voltage of component  $T$  during an interruption test. At time  $t = 0$  ms, the mechanical breaker is closed,  $S_1$  is opened,  $S_2$  is closed, and in this situation, capacitor  $C$  is connected in parallel to the input source. At time  $t_1 = 1.4$  ms, the opening button is pressed, and a trip command is sent to the mechanical breaker. At time  $t_2 = 4.6$  ms, the hysteresis control of the current of the mechanical breaker is activated. Switch  $S_2$  is opened, and switch  $S_1$  is switched on and off in order to maintain the mechanical breaker current in a range near zero. In this way, at time  $t_3 = 5.1$  ms, the mechanical breaker can open with a current near zero with a limited arc, and finally, at time  $t_4 = 5.6$  ms, the switch  $S_1$  can be opened. During the phase  $t_2 - t_3$ , the current is provided by capacitor  $C$ .

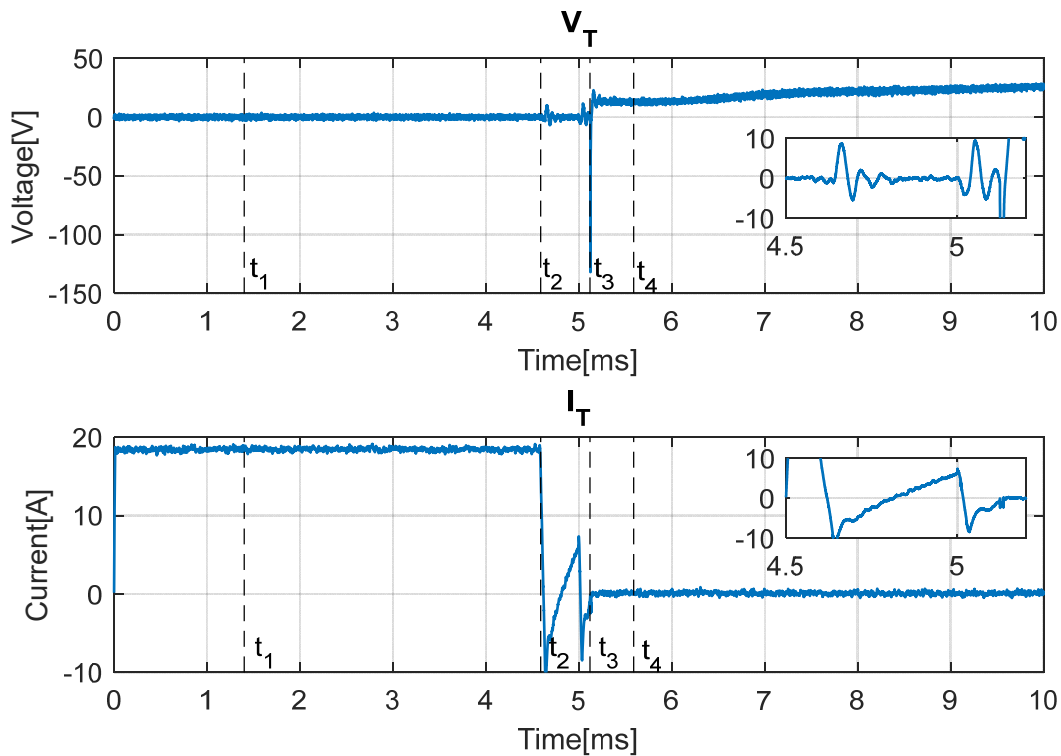


Fig. 11. Resistive load interruption test: mechanical breaker voltage and current

Looking at Fig. 12, it is also possible to see that the output voltage, and consequently the output current, increase during the phase between  $t_2$  and  $t_3$  because of the insertion of the capacitor  $C$ . In addition, the switching of the electronic components creates high frequency oscillations on the output voltage that are limited in amplitude. The peak of overvoltage is equal to 225 V that represent only the 12.5 % of the nominal voltage.

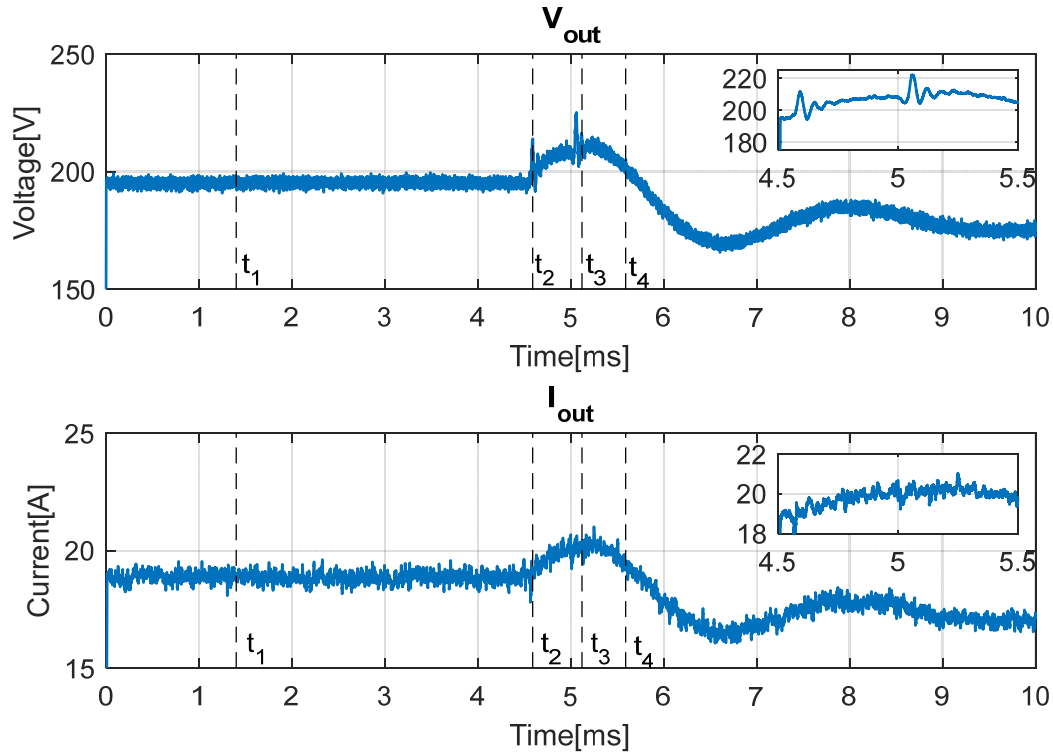


Fig. 12. Resistive load interruption test: load and capacitor current

#### b. Resistive fault interruption test

The performance of the HCB was also verified during a fault condition. An experiment was performed with the same system configuration described above. The opening command was triggered, in this case, at a preset output current level equal to 60 A. Fig. 13 shows the voltage and current of the mechanical circuit breaker. At time  $t_1 = 1.75$  ms, the fault is recognized by the control of the HCB, and the sequence presented above is activated. At time  $t_2 = 5.00$  ms, switch  $S_1$  starts to modulate, and the current in mechanical breaker  $T$  is maintained near zero until it opens its contact at time  $t_3 = 5.55$  ms. Starting from this moment, the output current, as shown in Fig. 14, is provided through  $S_1$  until its opening at  $t_4 = 6.00$  ms, and then only by the capacitor through diode  $D_2$ . After the fault, the output current decreases because of the voltage drop on the inductances. The output capacitor is therefore necessary to provide the initial peak current triggering the opening of the hybrid breaker.

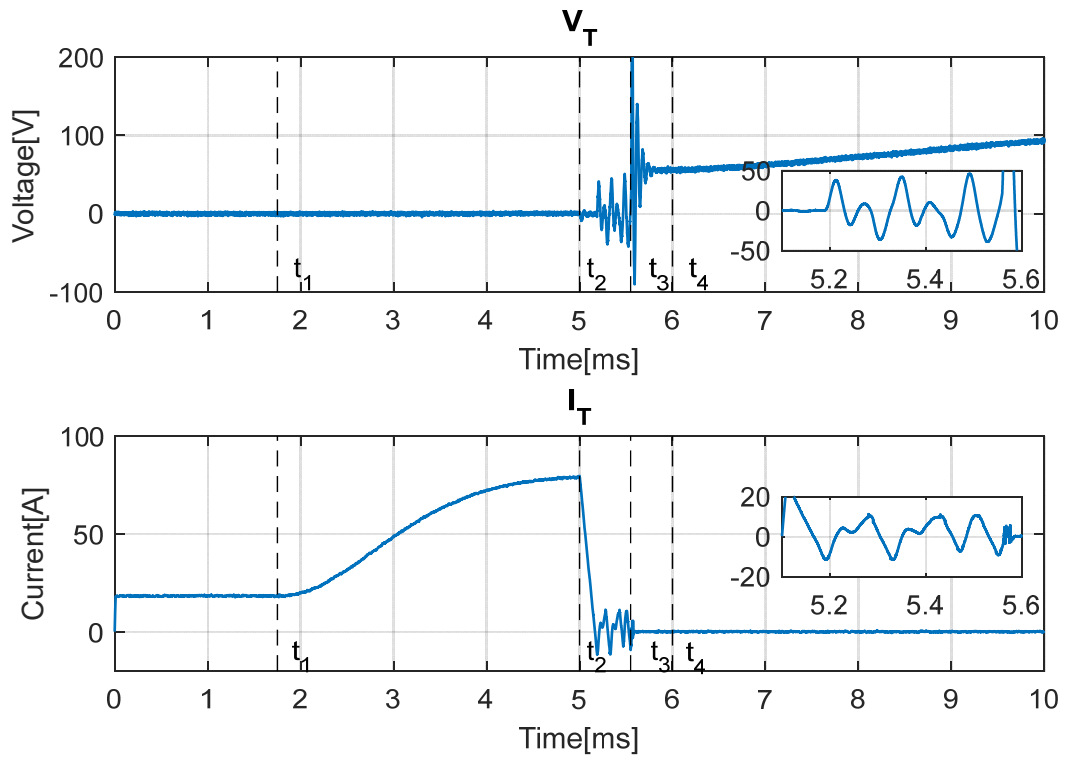


Fig. 13. Resistive fault interruption test: mechanical breaker voltage and current

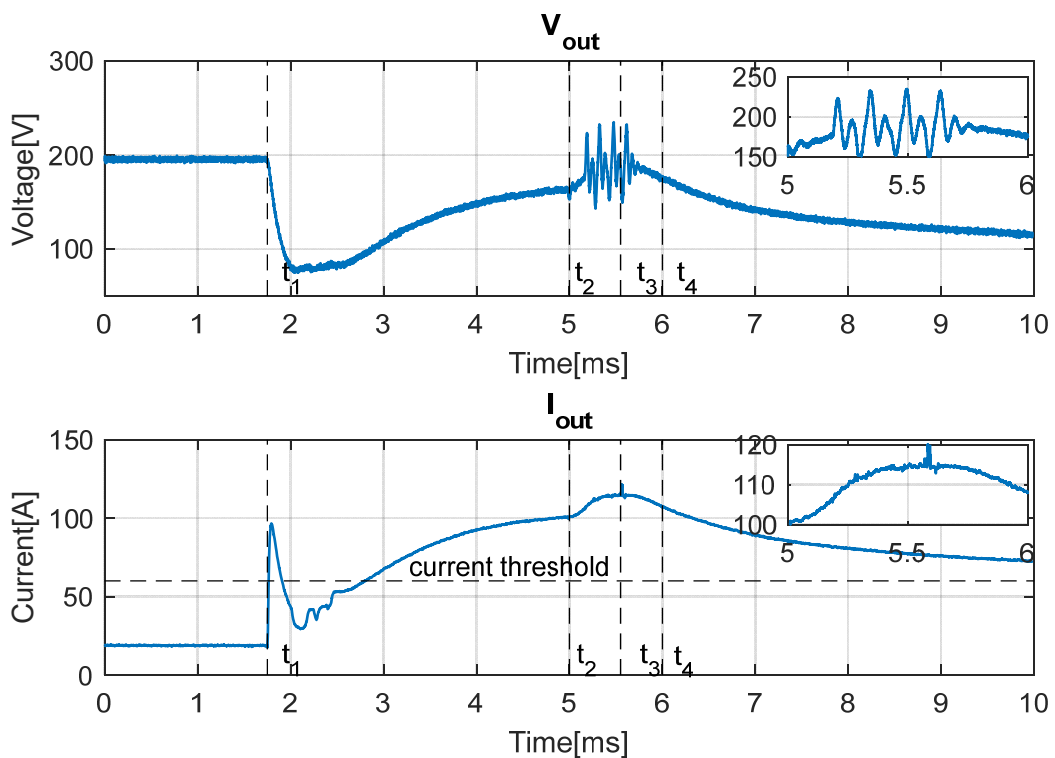


Fig. 14. Resistive fault interruption test: load voltage and current

It is worth noting that, also in case of the short circuit, the insertion of the capacitor  $C$  and the switching of the component  $S_1$ , create an overvoltage on the output terminal of the HCB are limited to 16.5 % of the nominal voltage.

The output voltage oscillation causes only a very small perturbation on the output current since the line and the load have parasitic inductances that limit it

The test results demonstrated that the proposed HCB and its control are also able to operate during a fault with a limited arc on the mechanical breaker. This makes it possible to obtain a long lifetime for this component. In addition, the HCB has the ability to open under a short circuit without damage. The voltage applied to components  $S_1$  and  $S_2$ , as shown in Fig. 15, are about two times the nominal voltage of the grid. This overvoltage is due to the parasitic inductance of the input circuit and can be reduced through the use of a capacitance connected in parallel with the input of the breaker. The current flowing through  $C$  is equal to the current flowing in the turned on switch.

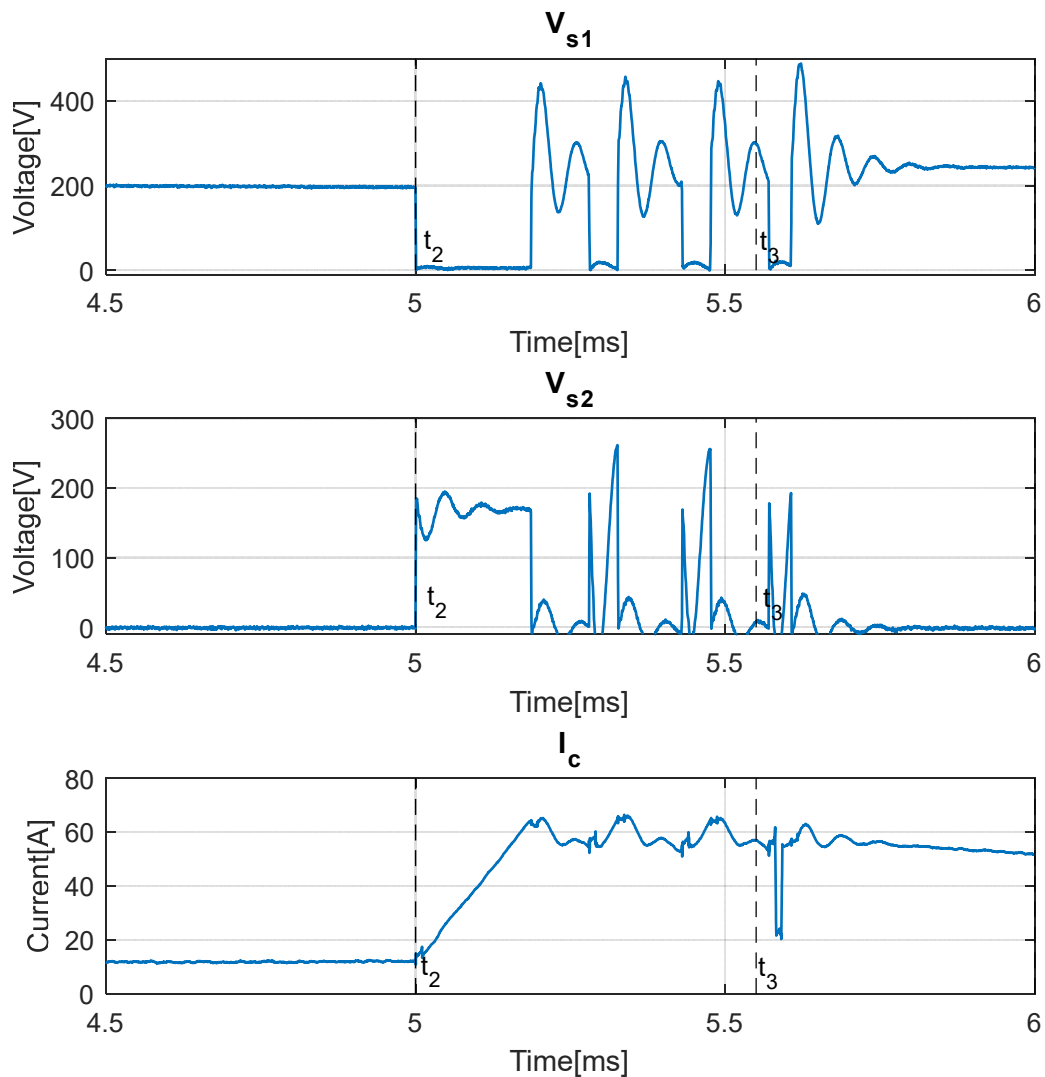


Fig. 15. Resistive fault interruption test: voltage applied to switches  $S_1$  and  $S_2$  and current in capacitor  $C$

### c. Performance analysis

To analyze the performance of the realized hybrid circuit breaker in terms of energy efficiency, additional tests were performed, in order to evaluate the internal resistance of the breaker. In the test, the prototype was operated at the

nominal voltage and current for two hours, in order to reach a steady **state temperature**. **After that**, by means of a Power Analyzer Hioki PW3390, the current and the voltage at the input and output port were measured to estimate the **internal resistance of the HCB components which was 33 mΩ**. This resistance is due to the inductance  $L$  of 400  $\mu\text{H}$ , that has an internal resistance of 6 mΩ, and to the output inductance  $L_{out}$  of 1.8 mH, that present 27 mΩ of internal resistance. It is worth noting that for the proposed circuit breaker, the choice of the mechanical breaker has a strong influence on the losses of the HCB. With a fast MCB, like the one presented in [24], and considering a total breaking time of 1 ms, in order to identify the fault location, the inductance  $L$  and  $L_{out}$  can be reduced respectively to 200  $\mu\text{H}$  and to 600  $\mu\text{H}$ . In this condition, it is expected that the total resistance reaches values near 10 mΩ.

However, with reference to a solid state circuit breaker, the conduction losses depends on the type of power semiconductor device used. IGBT is a bipolar device and can be modeled as the series of the on-state voltage that cause conduction losses. On the other hand, MOSFET is a unipolar device and the conduction losses depend only on the on-state resistance. Furthermore, the MOSFET resistance have a positive temperature coefficient and consequently the on-state resistance increases of 2-3 times passing from the reference temperature (25°C) to the maximum temperature. In addition semiconductor wafer of SSCBs may break down due to overvoltages and overcurrents [26]. This is true in particular for SiC MOSFET that have low short circuit withstand capability, compared with Si IGBTs and MOSFETs. In particular, the typical short circuit withstand time of SiC MOSFETs is normally on the order of 1  $\mu\text{s}$  for low voltage application and 10  $\mu\text{s}$  for medium voltage [37]. This requires a faster response time to guarantee the operation in the safe operation area and avoid overcurrent condition that has negative impact on the long term stability of the device.

To compare the losses of the proposed HCB with the losses of a comparable electronic circuit breaker in Table 2 different types of power semiconductor devices (IGBT, Si MOSFET, SiC MOSFET and SiC JFET), suitable for the voltage and current of the HCB, are collected. As shown **in** this table, the losses of the proposed HCB are less than the losses of a pure electronic breaker. In particular, considering a fast MCB, the losses are five times less than the losses of the best solid state circuit breaker.

Table 2 Comparison in terms of losses between the proposed HCB and some typology of Transistor

Component	Manufacturer	Forward Voltage [V]	Internal Resistance [mΩ]	Losses @ 20 A [W]
Hybrid Circuit Breaker	/	/	33	13.2
Hybric Circuit Breaker with a fast MCB [24]	/	/	10	4
Si IGBT SKM 75GB063D	Semikron	1.05	14	26.6
Si MOSFET VS-FA72SA50LC	Vishay	/	80	32
SiC JFET UJN1205K	UnitedSiC	/	45	18
SiC MOSFET SCTWA50N120	STMicroelectronics	/	69	27.6

To verify the performance of the proposed HCB in comparison with the MCB in terms of lifetime, it's necessary to analyze the voltage and the current applied to the mechanical breaker during the interruption test. Fig. 16 and Fig. 17 show the trends of voltage and current for the mechanical circuit breaker during a load interruption and a fault interruption in the case of HCB and MCB. In the case of MCB, the voltage applied to the mechanical breaker increases to high value during the interruption process and consequently the current decreases, while in the case of HCB, the current tends to zero in a very fast way thanks to the switching of  $S_1$  and the voltage is limited to tens of volt. As a consequence, the energy associated to the release of the mechanical breaker in the HCB is much lower than the one of the MCB. In Table 3 the energies associated to the interruption processes, dissipated by the mechanical breaker, are compared for the MCB and the HCB.

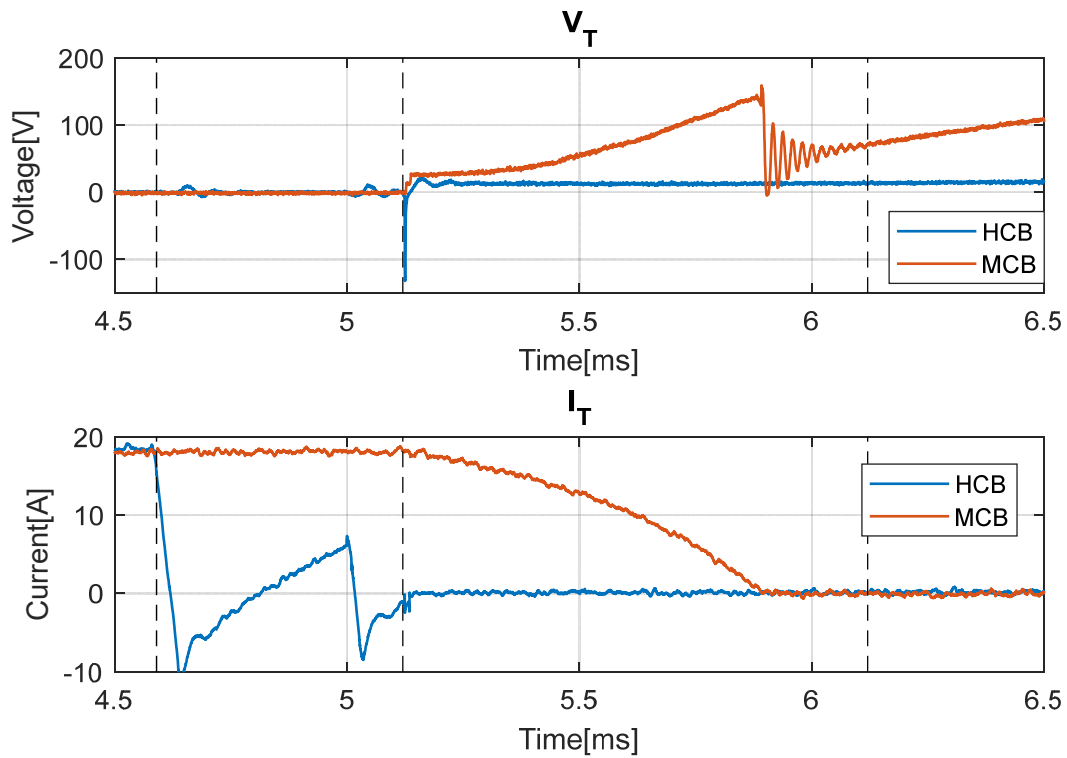


Fig. 16. Resistive load interruption test: comparison between the voltage and the current in the mechanical circuit breaker for the HCB and only the MCB

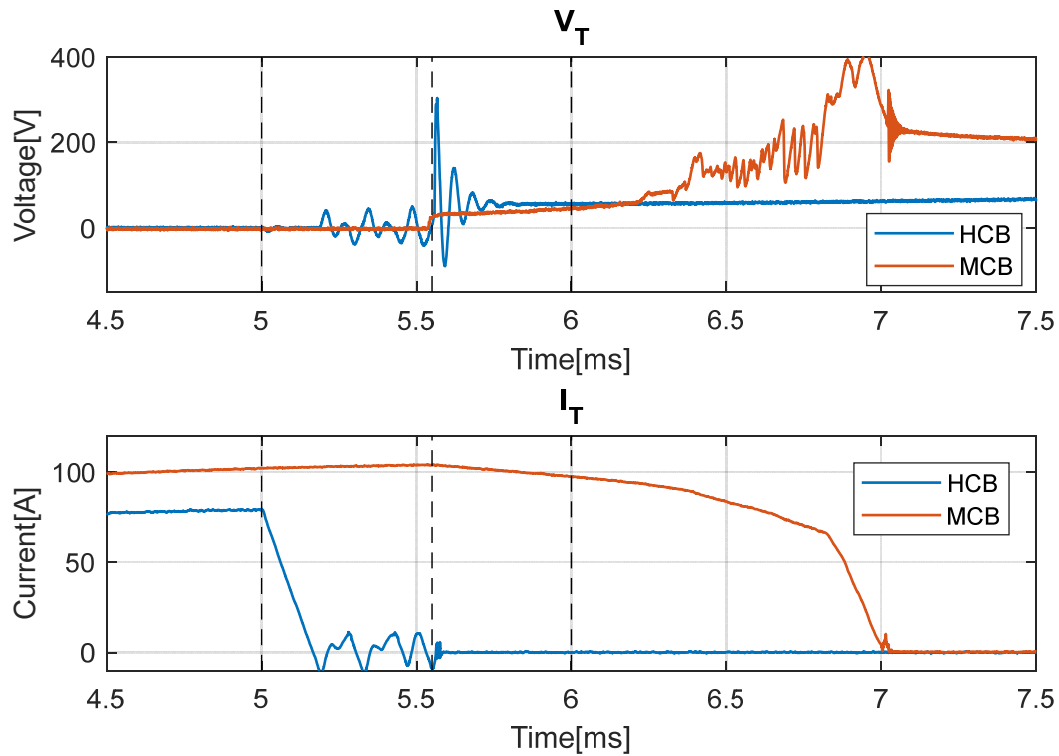


Fig. 17. Resistive fault interruption test: comparison between the voltage and the current in the mechanical circuit breaker for the HCB and only the MCB

Table 3 Comparison between the proposed HCB and MCB in terms of energies dissipated by the mechanical breaker during the interruption process

	Energy dissipated during the interruption process	
	MCB	HCB
Resistive load interruption of 11 $\Omega$	442.0 mJ	3.3 mJ
Resistive fault interruption of 2 $\Omega$	12200 mJ	14.0 mJ

Considering the life characteristic as a function of the current for the adopted mechanical circuit breaker [38] shown in Fig. 18, it is possible to evaluate the estimated number of cycles this component can perform in case of HCB and MCB configurations.

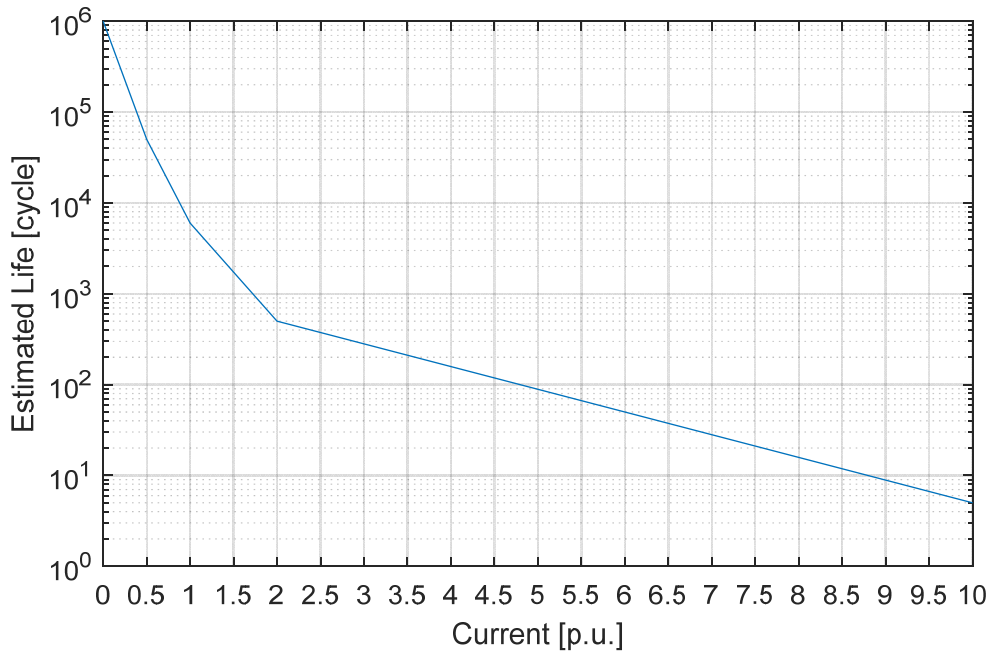


Fig. 18. Lifetime characteristic of the mechanical circuit breaker

For a current equal to the nominal current (20 A) the MCB can perform 6000 cycles, while with a current of about 10 A, that is the current threshold in the HCB, the MCB can perform 50000 cycles. In case of fault interruption with a current of 100 A, the estimated life is about 100 cycles, while resorting to the HCB is equal to 50000 cycles. It's worth noting that the values provided by the manufacturer are related to current interruptions with arc formation. The proposed HCB however reduces the arc time and consequently the energy dissipated by the mechanical breaker. This put in evidence that the expected lifetime of the mechanical breaker used in the HCB could be higher than the values provided by the manufacturers.

## 6. Conclusion

In recent years, several studies have been conducted dealing with protection devices for low-voltage DC systems. The solutions can be divided in three categories: i) those based on mechanical improvements to extinguish the electric arc, ii) those consisting of the use of innovative electronic switches with very low voltage drops, and iii) those that use hybrid topologies, including static and mechanical breakers. In this paper, an innovative topology for a hybrid low-voltage DC breaker was proposed. In the proposed solution, a conduction operation is achieved by means of a fast mechanical breaker, ensuring a very low voltage drop and consequent low conduction losses. In contrast, the opening maneuver is achieved by activating an electronic power switch that keeps the current in the mechanical breaker close to zero until this last one opens its contacts. In this way, the mechanical device has to break a very low current with reduced or no-formation of an arc, and consequently a very long lifetime. The proposed topology is designed to also operate correctly in the case of a short circuit. In this case, it is capable of limiting the rising of the current (due to the



short circuit) for the whole time necessary to complete the opening operation. In this way, the proposed hybrid DC breaker can be used to protect any device and, in particular, power electronic converters that are not overloadable.

In this paper, a new topology was proposed, and its working principle was theoretically analyzed. Then, the dimensioning of all the components of the device were studied to make the breaker capable of also working in the case of a short circuit. Finally, the results of experimental tests performed on a dedicated prototype were presented and discussed. It was found to be opportune to use very fast mechanical breakers to reduce the size and weight of each component. They operate by opening very low currents, but a smaller hybrid device can be designed if they are faster at opening their contacts. The proposed solution is a step forward for the existing hybrid solutions because it is the first one that allows both normal and short circuit operations without damage or extra-ageing of the device.

## References

- [1] J.J. Justo, F. Mwasilu, J. Lee, J.Jung, "AC-microgrids versus DC-microgrids with distributed energy resources: A review, *Renewable and Sustainable Energy Reviews*", Volume 24, August 2013, Pages 387-405
- [2] T. Kaipia, P. Salonen, J. Lassila, and J. Partanen, "Application of low voltage DC-distribution system—A techno-economical study," in *International Conference and Exhibition on Electricity Distribution, 2007*, pp. 1–4.
- [3] M. E. Baran and N. R. Mahajan, "DC Distribution for Industrial Systems: Opportunities and Challenges," *IEEE Trans. Ind. Appl.*, vol. 39, no. 6, pp. 1596–1601, Nov./Dec. 2003.
- [4] P. Nuutinen, T. Kaipia, P. Peltoniemi, A. Lana, A. Pinomaa, P. Salonen, J. Partanen, J. Lohjala, and M. Matikainen, "Experiences from use of an LVDC system in public electricity distribution," in *22nd International Conference and Exhibition on Electricity Distribution (CIRED)*. IET, 2013, pp. 1–4.
- [5] S. Grillo, V. Musolino, L. Piegari, E. Tironi, and C. Tornelli, "DC Islands in AC Smart Grids," *IEEE Trans. Power Electron.*, vol. 29, no. 1, pp. 89–98, Jan. 2014.
- [6] T. Dragicevic, J. C. Vasquez, J. M. Guerrero and D. Skrlec, "Advanced LVDC Electrical Power Architectures and Microgrids: A step toward a new generation of power distribution networks," in *IEEE Electrification Magazine*, vol. 2, no. 1, pp. 54-65, March 2014.
- [7] R. M. Cuzner and G. Venkataramanan, "The status of DC micro-grid protection," in *Industry Applications Society Annual Meeting, 2008. IAS'08*. IEEE, pp. 1–8, IEEE, 2008.
- [8] A. A. S. Emhemed and G. M. Burt, "An Advanced Protection Scheme for Enabling an LVDC Last Mile Distribution Network," in *IEEE Transactions on Smart Grid*, vol. 5, no. 5, pp. 2602-2609, Sept. 2014.
- [9] D. Salomonsson, L. Soder and A. Sannino, "Protection of Low-Voltage DC Microgrids," in *IEEE Transactions on Power Delivery*, vol. 24, no. 3, pp. 1045-1053, July 2009.
- [10] A. Emhemed and G. Burt, "The effectiveness of using IEC61660 for characterising short-circuit currents of future low voltage DC distribution networks," in *Proc. Int. Conf. Exhib. Electr. Distrib. (CIRED)*, Stockholm, Sweden, Jun. 2013, pp. 1–4.
- [11] W. Rieder, "Circuit breakers Physical and engineering problems I—Fundamentals," *IEEE Spectr.*, vol. 7, no. 7, pp. 35–43, Jul. 1970.
- [12] W. Rieder, "Circuit breakers Physical and engineering problems II—Design considerations," *IEEE Spectr.*, vol. 7, no. 8, pp. 90–94, Aug. 1970.
- [13] W. Rieder, "Circuit breakers Physical and engineering problems III—Arc-medium considerations," *IEEE Spectr.*, vol. 7, no. 9, pp. 80–84, Sep. 1970.
- [14] Mustafa Farhadi, Osama A. Mohammed, Protection of multi-terminal and distributed DC systems: Design challenges and techniques, *Electric Power Systems Research*, Volume 143, 2017, Pages 715-727
- [15] H. Pugliese and M. von Kannewurff, "Discovering DC: A Primer on dc Circuit Breakers, Their advantages, and Design," in *IEEE Industry Applications Magazine*, vol. 19, no. 5, pp. 22-28, Sept.-Oct. 2013
- [16] C. Meyer, S. Schroder and R. W. De Doncker, "Solid-state circuit breakers and current limiters for medium-voltage systems having distributed power systems," in *IEEE Transactions on Power Electronics*, vol. 19, no. 5, pp. 1333-1340, Sept. 2004
- [17] F. Liu, W. Liu, X. Zha, H. Yang and K. Feng, "Solid-State Circuit Breaker Snubber Design for Transient Overvoltage Suppression at Bus Fault Interruption in Low-Voltage DC Microgrid," in *IEEE Transactions on Power Electronics*, vol. 32, no. 4, pp. 3007-3021, April 2017
- [18] J. Magnusson, R. Saers, L. Liljstrand and G. Engdahl, "Separation of the Energy Absorption and Overvoltage Protection in Solid-State Breakers by the Use of Parallel Varistors," in *IEEE Transactions on Power Electronics*, vol. 29, no. 6, pp. 2715-2722, June 2014
- [19] A. M. S. Atmadji and J. G. J. Sloot, "Hybrid switching: a review of current literature," *Energy Management and Power Delivery*, 1998. Proceedings of EMPD '98. 1998 International Conference on, 1998, pp. 683-688 vol.2.
- [20] A. Shukla and G. D. Demetriades, "A Survey on Hybrid Circuit-Breaker Topologies," in *IEEE Transactions on Power Delivery*, vol. 30, no. 2, pp. 627-641, April 2015
- [21] B. Roodenburg, A. Taffone, E. Gilardi, S. M. Tenconi, B. H. Evenblij and M. A. M. Kaanders, "Combined ZVS--ZCS topology for high-current direct current hybrid switches: design aspects and first measurements," in *IET Electric Power Applications*, vol. 1, no. 2, pp. 183-192, March 2007.
- [22] C. M. Franck, "HVDC Circuit Breakers: A Review Identifying Future Research Needs," in *IEEE Transactions on Power Delivery*, vol. 26, no. 2, pp. 998-1007, April 2011
- [23] P. J. Theisen, et. al., 270-V DC Hybrid Switch, *IEEE Trans. On Components, Hybrids and Manufacturing Technology*. Vol. CHMT-9. No. 1, March 1986, p. 97-100.

- [24] J. M. Meyer and A. Rufer, "A DC hybrid circuit breaker with ultra-fast contact opening and integrated gate-commutated thyristors (IGCTs)," in *IEEE Transactions on Power Delivery*, vol. 21, no. 2, pp. 646-651, April 2006
- [25] S. Roy, D. Kanabar, C. Dodiya and S. Pradhan, "Development of a Prototype Hybrid DC Circuit Breaker for Superconducting Magnets Quench Protection," in *IEEE Transactions on Applied Superconductivity*, vol. 24, no. 6, pp. 1-6, Dec. 2014
- [26] D. Keshavarzi, E. Farjah and T. Ghanbari, "Hybrid DC Circuit Breaker and Fault Current Limiter With Optional Interruption Capability," in *IEEE Transactions on Power Electronics*, vol. 33, no. 3, pp. 2330-2338, March 2018
- [27] A. Hassanpoor, J. Häfner and B. Jacobson, "Technical Assessment of Load Commutation Switch in Hybrid HVDC Breaker," in *IEEE Transactions on Power Electronics*, vol. 30, no. 10, pp. 5393-5400, Oct. 2015
- [28] X. Song, C. Peng and A. Q. Huang, "A Medium-Voltage Hybrid DC Circuit Breaker, Part I: Solid-State Main Breaker Based on 15 kV SiC Emitter Turn-OFF Thyristor," in *IEEE Journal of Emerging and Selected Topics in Power Electronics*, vol. 5, no. 1, pp. 278-288, March 2017
- [29] C. Peng, X. Song, A. Q. Huang and I. Husain, "A Medium-Voltage Hybrid DC Circuit Breaker—Part II: Ultrafast Mechanical Switch," in *IEEE Journal of Emerging and Selected Topics in Power Electronics*, vol. 5, no. 1, pp. 289-296, March 2017
- [30] J. Zyborski, T. Lipski, J. Czucha and S. Hasan, "Hybrid arcless low-voltage AC/DC current limiting interrupting device," in *IEEE Transactions on Power Delivery*, vol. 15, no. 4, pp. 1182-1187, Oct 2000.
- [31] Tsegay Gebremedhin Hailu, Laurens Mackay, Laura M. Ramirez-Elizondo & Jan A. Ferreira (2017) Voltage Weak DC Distribution Grids, *Electric Power Components and Systems*, 45:10, 1091-1105
- [32] S. Anand and B. G. Fernandes, "Reduced-Order Model and Stability Analysis of Low-Voltage DC Microgrid," in *IEEE Transactions on Industrial Electronics*, vol. 60, no. 11, pp. 5040-5049, Nov. 2013
- [33] D. Jovicic, W. Lin, S. Nguéfeu and H. Saad, "Low-Energy Protection System for DC Grids Based on Full-Bridge MMC Converters," in *IEEE Transactions on Power Delivery*, vol. 33, no. 4, pp. 1934-1943, Aug. 2018
- [34] C. Peng, I. Husain, A. Q. Huang, B. Lequesne and R. Briggs, "A Fast Mechanical Switch for Medium-Voltage Hybrid DC and AC Circuit Breakers," in *IEEE Transactions on Industry Applications*, vol. 52, no. 4, pp. 2911-2918, July-Aug. 2016.
- [35] M.A. Sanchez, Dynamics of an ultra-fast Thomson-actuated HVDC breaker, MSc thesis at KTH Industrial Engineering and Management, June 2017, available at <https://kth.diva-portal.org/smash/get/diva2:1113124/FULLTEXT01.pdf>, accessed on June 19th 2018
- [36] D. Ronchegalli and R. Lazzari, "Development of the control strategy for a direct current microgrid: A case study," *2016 AEIT International Annual Conference (AEIT)*, Capri, 2016, pp. 1-6
- [37] F. F. Wang and Z. Zhang, "Overview of silicon carbide technology: Device, converter, system, and application," in *CPSS Transactions on Power Electronics and Applications*, vol. 1, no. 1, pp. 13-32, Dec. 2016
- [38] available online at [http://www.te.com/commerce/DocumentDelivery/DDEController?Action=srchrtv&DocNm=5-1773450-5\\_Section7&DocType=CS&DocLang=EN](http://www.te.com/commerce/DocumentDelivery/DDEController?Action=srchrtv&DocNm=5-1773450-5_Section7&DocType=CS&DocLang=EN), accessed on June 1st, 2018